ACS OMEGA

http://pubs.acs.org/journal/acsodf

Article

Doped SnO_2 Nanomaterials for E-Nose Based Electrochemical Sensing of Biomarkers of Lung Cancer

Zeenat Khatoon, Hassan Fouad,* Othman Y. Alothman, Mohamed Hashem, Zubaida A. Ansari, and Shafeeque Ahmed Ansari*

Cite This: *ACS Omega* 2020, 5, 27645−27654

Read Online

ACCESS | Metrics & More | Article Recommendations | Supporting Information

ABSTRACT: Lung cancer detection includes detection of a pattern formed by multiple volatile organic compounds. An individual material has limited selectivity and hence requires tailoring to improve the selectivity and sensing properties. An electronic nose (e-nose) is a concept/device that can help in achieving selectivity and specificity for multiple volatile organic compounds at the same time by using an array of sensors. In this paper, Co and Ni doping in tin oxide was used to investigate as a sensor material for e-nose development. These were synthesized using a sol−gel method and were characterized for structural, morphological, and elemental assessment using X-ray diffraction, field emission scanning electron microscopy, and Fourier transform infrared spectroscopy, which indicated the formation of the composite nanomaterial of SnO_2. These synthesized materials were then used as a working electrode in the form of a screen-printed electrode to determine 1-propanol and isopropyl alcohol (IPA) sensing characteristics. Electrochemical characterization was done by cyclic voltammetry (CV) and electrochemical impedance spectroscopy. In the case of CV studies, well-defined and distinct redox peaks are observed at different potential values indicating the changes due to the dopants. Ni doping in SnO_2 shows the highest sensitivity of 2.99 μA/ppb for isopropyl alcohol and 3.11 for 1-propanol, within the detection range. Furthermore, Co−SnO_2 shows selectivity for IPA, while Ni−SnO_2 is selective to 1-propanol against all other volatile compounds analyzed.

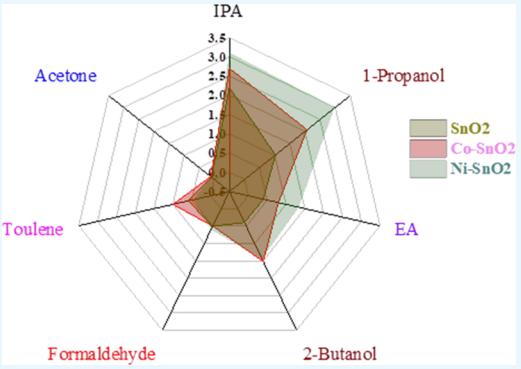

1. INTRODUCTION

Cancer has become the second leading cause of death globally following the cardiovascular disease. According to the World Health Organization, one in six deaths is due to cancer. Survival rates vary drastically subject to the type of cancer, its severity, and how early it is detected. Among various types of cancer, lung cancer (LC) has emerged as one of the vulnerable types, leading to death universally irrespective of the gender. It is yet a big challenge to detect LC at an early stage to significantly enhance treatment success and survival rate. Recently, development of an inexpensive, convenient, and non-invasive technique based on the analysis of multiple volatile organic compounds (VOCs) that originate from diseased cells to improve cancer detection has drawn increasing research attention worldwide,[1,2] which can serve as a good tool for early diagnosis and treatment. In terms of biochemistry, VOCs can offer an insight into the various ongoing physiological processes in both healthy and diseased humans. The analysis of VOCs in exhaled air during breathing is an evolving method for the screening and diagnosis of the LC disease.[3−9] The early studies suggest LC-specific VOCs can be detected not only in the exhaled air but also in the headspaces of blood from an LC patient.[10] It has been reported that VOCs in exhaled air resulting from cancer patients exhibit specific patterns that are significantly different from healthy individuals.[11] According to a report, approximately 250 volatile organic compounds are present at ppm or ppb (parts per million/billion level) or a trace amount in the exhaled air that can be marked as a biomarker for the detection of lung cancer.[12]

The routine diagnosis of LC is based on a biochemical study, imaging, endoscopic, immunological, genomic, and pathological procedures having varied pros and cons including cost effectiveness, risk of life, etc. The traditional techniques are also utilized to detect these compounds, such as gas chromatography−mass spectrometry (GC−MS), selected-ion flow tube mass spectrometry (SIFT-MS), proton-transfer-reaction mass spectrometry (PTR-MS), and ion mobility, which are bulky, limited to lab use, requires skilled manpower, and are time consuming.[13−23] Recently, a wide range of gas sensors and sensor arrays are being developed for the ppm or ppb level detection of VOCs. Colorectal sensors, quartz

Received: August 31, 2020
Accepted: September 30, 2020
Published: October 14, 2020

https://dx.doi.org/10.1021/acsomega.0c04231
ACS Omega 2020, 5, 27645−27654

microbalance sensors, surface acoustic wave sensors, and chemiresistors or chemicapacitors are some of the development examples.[10,24] Furthermore, these sensors are nonspecific to detect multiple VOCs simultaneously in the complex VOC mixtures, which explains a need to develop an inexpensive, portable, highly sensitive/selective VOC detector.

An electrochemical technique provides an opportunity to develop such cheap, portable, and highly sensitive sensors for the detection of VOCs in the exhaled air and the combined analysis of VOCs emitted from different bodily sources.[25] These sensors are non-invasive and have the potential for VOC detection in exhaust mixtures due to their high selectivity and reliable performance under harsh conditions, e.g., high humidity and temperature. Implementation of an electrochemical approach will help in the development of a true point-of-care, non-invasive, easy to use, and relatively low-cost system like an electronic nose (e-nose), which can be an optimal screening tool for severe diseases including various types of cancer. However, there is a need to improve the sensitivity of electrochemical sensors to detect at the ppb level concentration of VOC markers in the exhaled air.[26] Various methods are investigated to improve the sensitivity of electrochemical sensors (such as UV-illumination that doubled the sensitivity of the sensor during detection) for an early stage disease diagnosis.[10,26]

Nanostructured semiconducting metal oxides (NMOs) are broadly used in chemiresistors as a sensing layer for oxidizing and reducing gases. Metal oxide (MO) nanoparticles are promising candidates for the sensor element design because of their extra ordinary surface properties, adjustable physicochemical property, and good stability.[26,27] NMOs have high density of trapped charged oxygen species, i.e., O_2^-, O^-, and O^{2-}, resulting into a surface charged layer in terms of electron-depletion or hole-accumulation subject to n-type and p-type, respectively. The gaseous phase reacts with the adsorbed negatively charged oxygen on the metal oxide surface, altering the surface-trapped charge density and the resistance. MOs owing to their more than one oxidation states are preferably used for gas sensing at the ppb level by controlling their shape, size, and composition.[28] Among these oxides, SnO_2, a wide band gap n-type semiconductor, is one of most investigated materials for gas sensing owing to its excellent physical, chemical, and thermal properties and chemical stability.[29] In addition, SnO_2 has nonstoichiometric oxygen composition, e.g., SnO and Sn_3O_4, which is an additional advantage in improving the sensing properties. However, undoped SnO_2 has a low electrical conductivity due to its intrinsically low carrier density and mobility; tailor-designed/engineered SnO_2 by doping or complexes with an advantage of chemical and/or morphological modifications and optimized operating conditions have been used for the detection of different gases.[28−32] Many metal elements are used as a dopant to improve the electrical and optical characteristics of SnO_2. Transition metals like Fe, Mn, Al, Co, Fe, Ni, Cu, Sb, etc. are preferably used as dopants due to their more than one oxidation states to improve the electrical and optical properties and also sensitivity for gases. Ni and Co metals are chosen in this work to control the electronic properties of SnO_2, which are among the best choices, other than this, they may play a role to control the synthesis of the SnO_2.

Choosing the sensing element for the formation of the array is the key to making the sensor array or an e-nose. Nanoparticles are one of the most important candidates for the sensor element design because of their extra ordinary surface properties, adjustable physicochemical property, and good stability. Based on this concept, in this paper, we prepared and used Co- and Ni-doped SnO_2 nanoparticles as the matrix for the electrochemical sensor to detect 1-propanol and isopropyl alcohol, VOC reported as biomarkers for lung cancer (LC).

2. RESULTS

2.1. Morphological and Structural Analysis. Figure 1(a−c) presents the FESEM micrographs of undoped SnO_2,

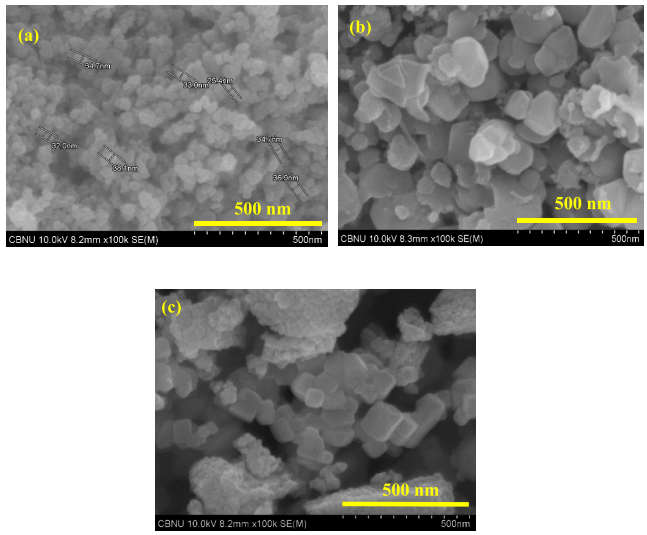

Figure 1. FESEM images showing the shape and size of the synthesized nanomaterial: (a) Undoped SnO_2, (b) Co−SnO_2, and (c)Ni−SnO_2.

Co−SnO_2, and Ni−SnO_2, respectively. Figure 1(a) revealed uniform-sized spherical particles of undoped SnO_2 (∼25 to 40 nm as shown on the image) evenly distributed over the surface. Figure 1(b,c) is the FESEM images of Ni−SnO_2 and Co−SnO_2, respectively, shows the agglomerated particles consisting of small spherical particles of about 15 to 20 nm in size; which are smaller than that of undoped SnO_2 (Figure 1(a)). Such morphology of fine particles would offer a higher surface to volume ratio and hence may improve the sensitivity due to the high density of adsorbed charged oxygen species, i.e., O_2^-, O^-, and O^{2-}. Furthermore, such morphology is favorable for adsorption-based sensors, as discussed in the later part of the manuscript.

Figure 2 depicts the XRD spectra of undoped SnO_2 (black), Co- (red), and Ni (green)-doped SnO_2. From the diffraction pattern, major characteristic peaks are oriented along (110), (101), (211), and (200), while minor peaks are oriented to (111), (220), (112), (301), (202), and (321) planes of SnO_2 with the structure of tetragonal rutile (a = 4.738 Å, c = 3.187 Å), matched with the standard JCPDS file number 41−1445. These peaks exist in all the samples, i.e., undoped and doped SnO_2; however, in Ni- and Co-doped samples, the intensity of peaks have reduced, while minor peaks in undoped SnO_2 are still seen as small humps. It is realized that the Ni and Co doping effect is not seen in the XRD pattern in the form of a distinct peak but is seen as changes in the peak width or changes in the crystalline nature of the synthesized material. This implies that undoped SnO_2 has larger crystal size and Ni

https://dx.doi.org/10.1021/acsomega.0c04231
ACS Omega 2020, 5, 27645−27654

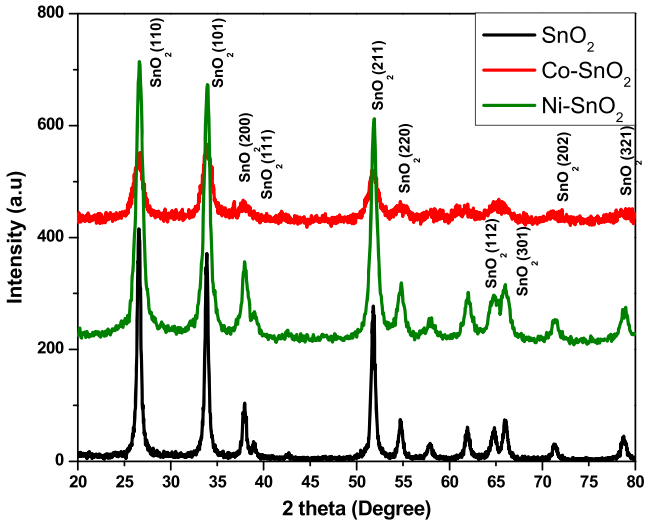

Figure 2. X-ray diffraction pattern (XRD) of undoped SnO_2, Co−SnO_2, and Ni−SnO_2.

and Co doping results in minimum-sized nanocrystals on synthesis, in agreement with the FESEM images shown in Figure 1. This is in agreement with the earlier reports for Ni- and Co-doped SnO_2.[30] The average crystallite size calculated using the Scherrer formula for the undoped, Co-, and Ni-doped SnO_2 is approximately 16 nm, 8 nm, and 11 nm following the same trend as observed from FESEM. There is no significant change in the lattice parameters and cell volume possibly due to the almost similar crystal radii of Sn (0.69 Å), Co (0.54 Å), and Ni (0.70 Å). No peak observed related to Ni and Co oxide or the composite phase confirms the low concentration of dopants in synthesized nanoparticles. The strain ε estimated using the Williamson−Hall (W-H) relation $\varepsilon = \beta_{hkl}/4\tan\theta$, in undoped SnO_2 is 0.7532, in Ni-SnO_2 it is 0.619, and it is 0.9984 in Co-SnO_2, which reveal that Co-doped SnO_2 possesses high strain that results in a reduced particle size as evident from FESEM.

Contact angle measurement was carried out to understand the surface wetting properties of the sensing electrode. Figure S1 (ESI) shows the images of water drops on undoped and doped SnO_2-coated glass slides. The contact angle (WCA) of the undoped SnO_2-coated glass slide is observed to be 51.9°. In Co-doped SnO_2, the contact angle reduced to 44.54°, i.e., surface wettability has increased while for Ni-doped SnO_2, the contact angle increased to 58.6°, which shows that the surface is more hydrophobic; this hydrophobic nature helps in self-cleaning of the sensor. Significantly, it demonstrates that the synthesis with dopants has resulted in a different surface wetting property, which is an advantageous thing for any adsorption-based sensor development.

2.2. UV−Vis and FTIR Study. Figure 3 shows the UV−vis spectra of undoped and doped SnO_2, which all exhibit the absorption peak centered at about 270 nm. Using UV−vis spectra, the Tauc's plot of sqrt ($\alpha h\nu$) vs energy (in eV) was plotted to estimate the value of the band gap. The band gap for SnO_2 is 3.69 eV and that for Ni-SnO_2 is 3.67 eV, whereas for Co−SnO_2 it is 3.45 eV. The doping results in the 0.54 to 6.5% reduction of the band gap for Ni−SnO_2 and Co−SnO_2, respectively. Such phenomenon is reported due to the Moss−Burstein effect in which the Fermi level shifts towards the high-energy side for doping of transition metals.

Figure 4 depicts the FT-IR spectra of calcined undoped SnO_2, Ni−SnO_2, and Co−SnO_2 obtained in the span of 600−

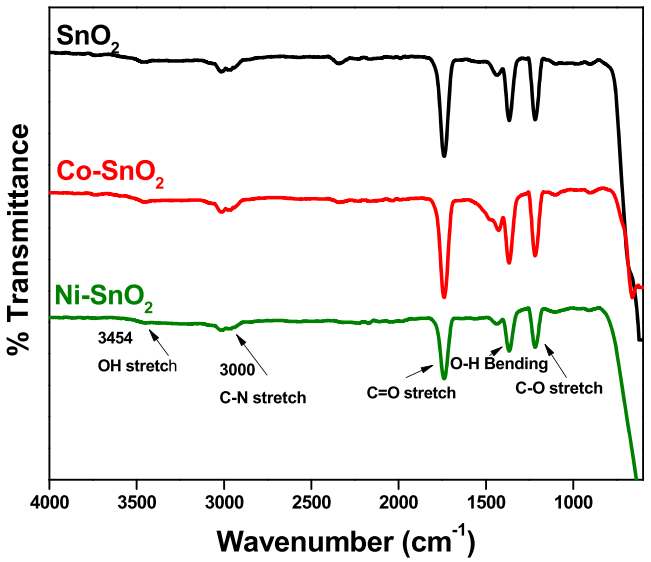

Figure 4. FT-IR spectrum of undoped and Co- & Ni-doped SnO_2 powder.

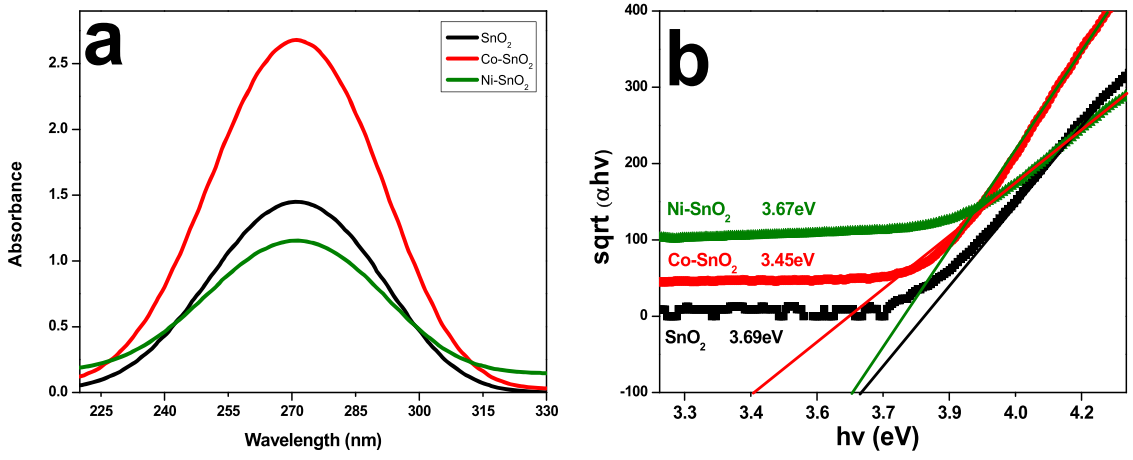

Figure 3. (a)UV−visible absorption spectra of synthesized nanoparticles, i.e., undoped SnO_2, Co−SnO_2, and Ni−SnO_2 powder; (b) Tauc plot for undoped SnO_2, Co−SnO_2, and Ni−SnO_2 powder.

https://dx.doi.org/10.1021/acsomega.0c04231
ACS Omega 2020, 5, 27645−27654

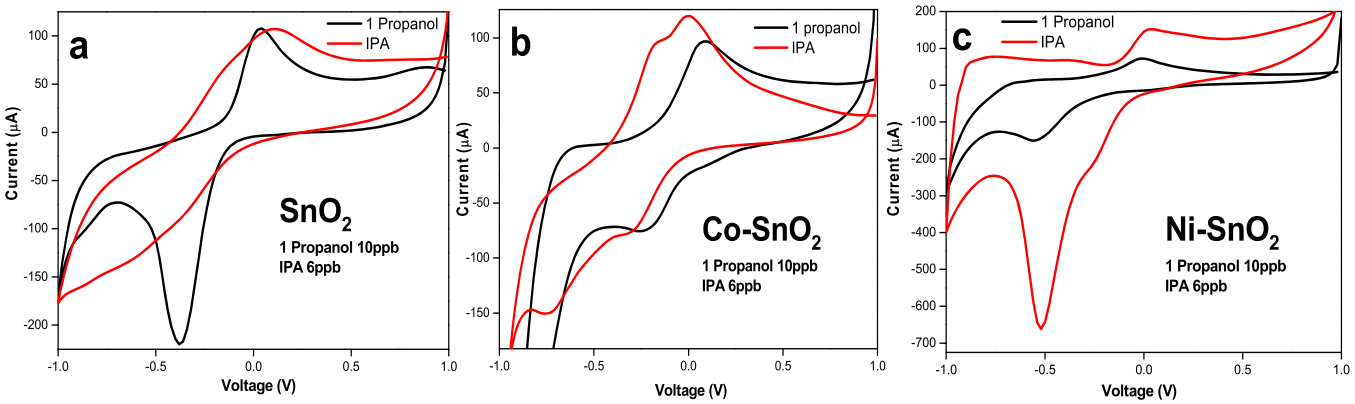

Figure 5. Cyclic voltammetry (CV) curves of the SnO_2, Co−SnO_2, and Ni−SnO_2 printed electrodes at 10 ppb of 1-propanol and 6 ppb of isopropyl alcohol.

4000 cm^{-1}. The wide vibration band observed at ∼600 cm^{-1} for all samples is the fingerprint region of MOs corresponding to the metal−oxygen stretching vibrations, and it confirms the synthesis of the MO compound. A band around 1200 cm^{-1} is due to C−O stretching, whereas a band around 1400 cm^{-1} is that of O−H bending vibrations. The strong band around 1690 cm^{-1} is due to C═O stretching. A broad weak vibration band at 3000 cm^{-1} is correlated to C−N stretching due to ammonia water used to neutralize pH. A very weak band around 3454 cm^{-1} is due to O−H stretching. The results indicate that the synthesized material has functional bands that may be useful for adsorption-based sensing studies.

2.3. Electrochemical Analysis. Figure 5 depicts the cyclic voltammograms obtained with 10 ppb of 1-propanol and 6 ppb of isopropyl alcohol with a sweeping voltage between −1 V to +1 V for the SPE prepared with undoped SnO_2, Co−SnO_2, and Ni−SnO_2. It can be seen that all samples exhibit a distinct redox reaction with different voltage and current values for both the analytes. The values of the difference between the redox potential obtained from Figure 5 for 1-propanol and isopropyl alcohol are listed in Table 1. For undoped SnO_2, the difference of the reduction and oxidation potential is 0.59 eV for 1-propanol and 0.68 eV for isopropyl alcohol, which suggests a reversible electrochemical reaction, as known in the literature. On the other hand, for doped SnO_2, the difference between the reduction and oxidation potential for both the analytes are between 0.30−0.5 eV (Table 1), which indicates the possibility of a quasi-reversible reaction.

Table 1. Details of the Peak Separation Potential as a Function of the Dopant

nanomaterials	1-propanol peak separation (V)	isopropyl alcohol peak separation (V)
SnO_2	0.59	0.68
Co−SnO_2	0.28	0.3
Ni−SnO_2	0.32	0.5

Figure 6 depicts the voltammogram obtained at a scan rate of 100 mV/sec for different concentrations of 1-proponal (0, 1, 5, 10, and 15 ppb) for undoped and doped SnO_2 wherein the change in the output as a function of concentration is visible.

Figure 6(a) reveals the CV curves for undoped SnO_2 at different concentrations of 1-propanol (0, 1, 5, 10, and 15 ppb) where a marginal increase in the oxidation peak current and the corresponding peak voltage is noticed. Similarly, the reduction peak current and peak voltage have marginally changed suggesting low sensitivity. Figure 6(b) shows the plot of the peak current as a function of concentration, which is used to calculate the sensitivity of the developed sensors, i.e., the slope of the curve is used as the sensitivity value (i.e., change in current per unit concentration). Sometimes, the area of the working electrode is also considered while calculating the sensitivity. The linearity for the oxidation peak current is 96%, while it is 90% for the reduction peak current over the detection range of the analyte (excluding the measurement in PBS: 0 ppb). It is worth noting that the sensor exhibited a linear response over the detection range used in the experiment.

In the case of Co−SnO_2 (Figure 6(c)), a noticeable reduction in the oxidation peak current and an increase in the reduction peak current are seen while the value of the redox peak potential remains the same at all concentrations. An increase in sensitivity (Figure 6(d)) compared to undoped SnO_2 is noted.

Ni−SnO_2 (Figure 6(e)) exhibited a maximum change in the redox current as a function of the 1-propanol concentration from 0−15 ppb. Figure 6(f) depicts the graph of the peak current as a function of the 1-propanol concentration with the sensitivity estimated from the oxidation peak current as 2.99 μA/ppb. This behavior may be correlated to both the smallest particle size (Figure 1(c)) and the high degree of mesoporosity arose due to the localized agglomeration of particles.

Similar characterization was carried out for the IPA analyte too using the SPE fabricated with undoped SnO_2, Co−SnO_2, and Ni−SnO_2, and the CV curves are shown in Figure 7. These were obtained at a scan rate of 100 mV/sec for different concentrations of IPA in the solution. The corresponding plot of the peak current as a function of the IPA concentration is also shown, which was used to estimate the sensitivity.

Figure 7(a) shows that the CV curves of undoped SnO_2 at different IPA concentrations from 2 to 10 ppb increased and exhibits an almost constant value of the oxidation/reduction peak current and peak voltage. The inset shows the magnified view of the peak area. The graph of the peak current as a function of concentration is monotonous (Figure 7(b)), which implies a significant change in the charge transfer resistance of the sensor during the electrochemical reaction, with a sensitivity of 2.2 μA/ppb over the detected range.

The voltammogram of Co−SnO_2 (Figure 7(c)) shows a noticeable increase of the oxidation current, whereas the reduction current is almost saturated beyond 6 ppb. The

https://dx.doi.org/10.1021/acsomega.0c04231
ACS Omega 2020, 5, 27645−27654

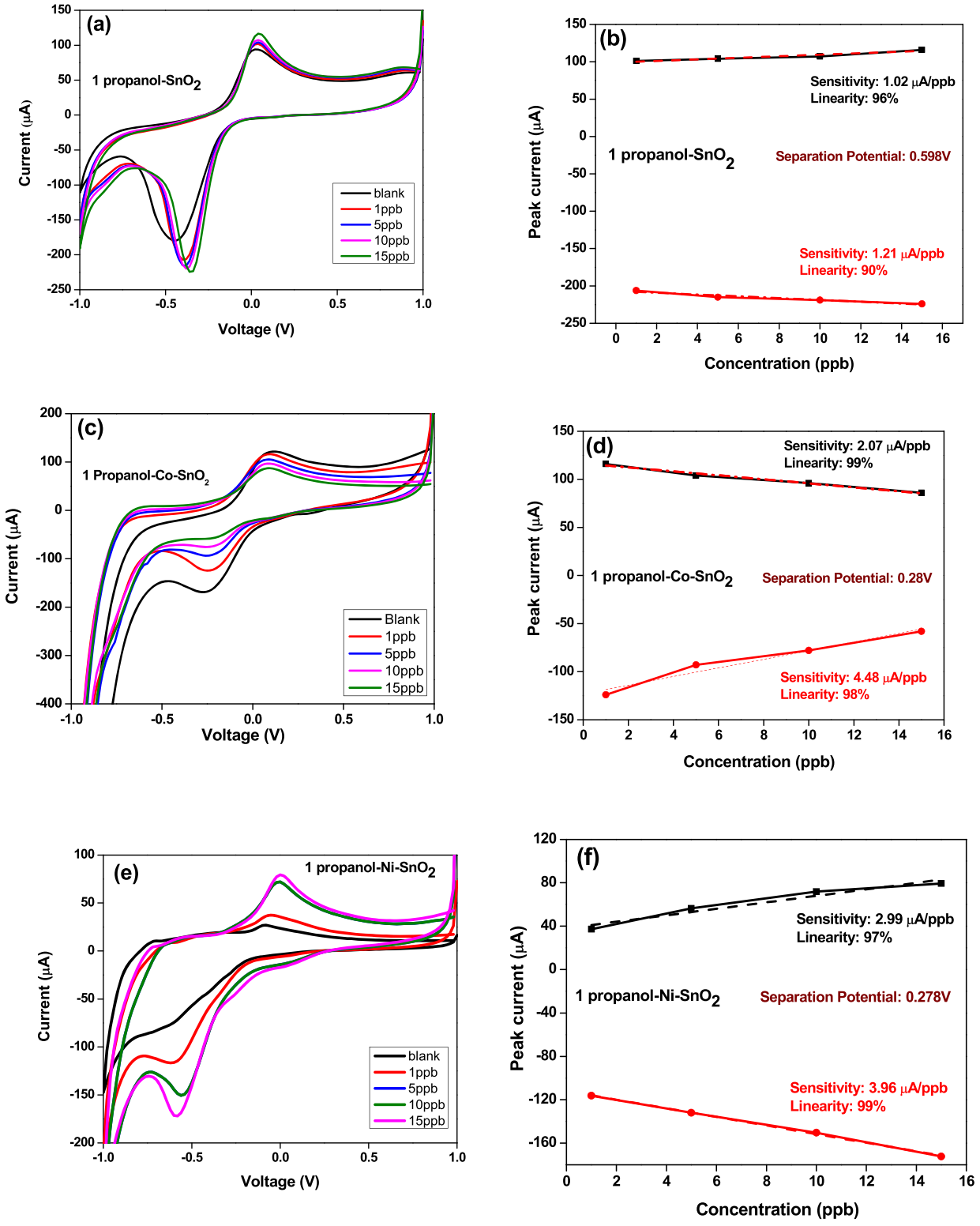

Figure 6. CV curves of the (a) SnO_2, (c) Co−SnO_2, and (e) Ni−SnO_2 modified electrodes at different concentrations (0−15 ppb) of 1-propanol. (b, d, f) Redox peak currents as a function of concentration. Dotted lines are the result of the best fitting.

corresponding graph of the peak current as a function of the IPA concentration (Figure 7(d)) depicts that the slope of the oxidation current is 2.75 μA/ppb, which almost same as that of the reduction peak current. In the case of Ni−SnO_2, linearity in response with the concentration is 99% with a sensitivity value of 3.11 μA/ppb (based on the oxidation peak current). As can be seen from Figure 7(e,f) the changes in the reduction peak current is much larger meaning a higher sensitivity value for the IPA concentration from 2 to 10 ppb (Figure 7(e)). The results obtained for 1-propanol and IPA are summarized as a bar graph in Figure 8, which indicates that Ni−SnO_2 exhibits the best sensitivity both for 1-propanol (Figure 8(a)) and IPA (Figure 8(b)). The LOD values estimated using a standard

https://dx.doi.org/10.1021/acsomega.0c04231
ACS Omega 2020, 5, 27645−27654

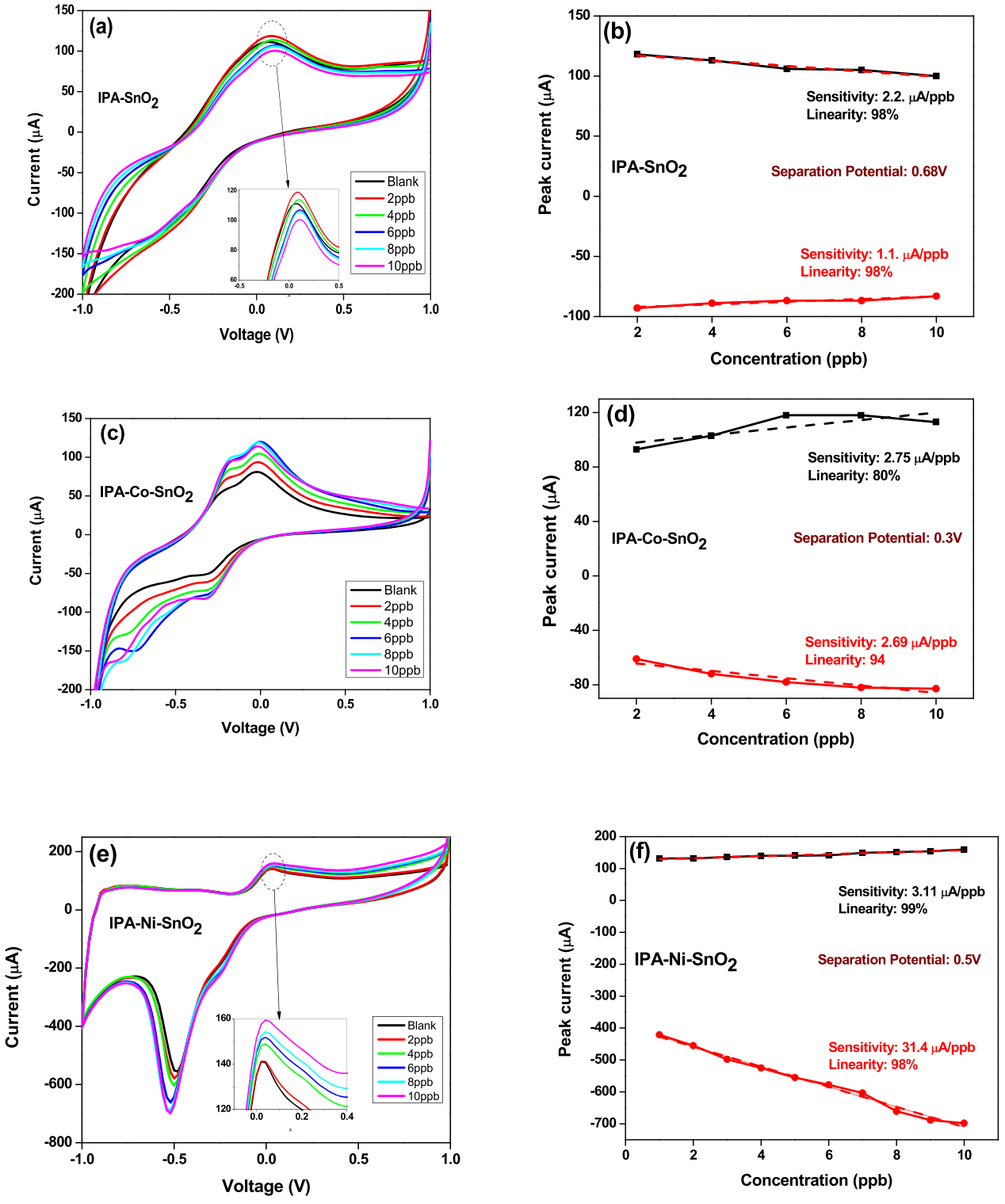

Figure 7. CV curves of the (a) SnO_2, (c) Co−SnO_2, and (e) Ni−SnO_2 modified electrodes at different concentrations (0−10 ppb) of isopropyl alcohol. (b, d, f) Redox peak currents as a function of concentration. Dotted lines are the result of the best fitting.

method (3.3σ/slope (sensitivity)) are shown in Figure 8 for the two analytes.

An e-nose based study was carried out to understand the highest sensitivity and selectivity. The cross sensitivity of all the sensors, i.e., SnO_2, Co−SnO_2, and Ni−SnO_2, were obtained for many other volatile organic compounds at different concentrations, such as 1−20 ppb of ethyl acetate, 1−15 ppb of 1-propanol, 10−600 ppb of acetone, 1−40 ppb of toluene, 2−10 ppb of isopropyl alcohol, 0.1−4 ppb of 1-butanol, and 1−10 ppb of formaldehyde. Figure 9 presents the radar chart that shows the selectivity of the developed sensor for different volatile organic compounds. The chart in Figure 9 clearly suggests that Ni−SnO_2 shows the highest sensitivity and selectivity for 1-propanol and then IPA against all other volatile compounds analyzed. However, Co−SnO_2 exhibits the highest sensitivity for IPA against all the volatile compounds tested. It

https://dx.doi.org/10.1021/acsomega.0c04231
ACS Omega 2020, 5, 27645−27654

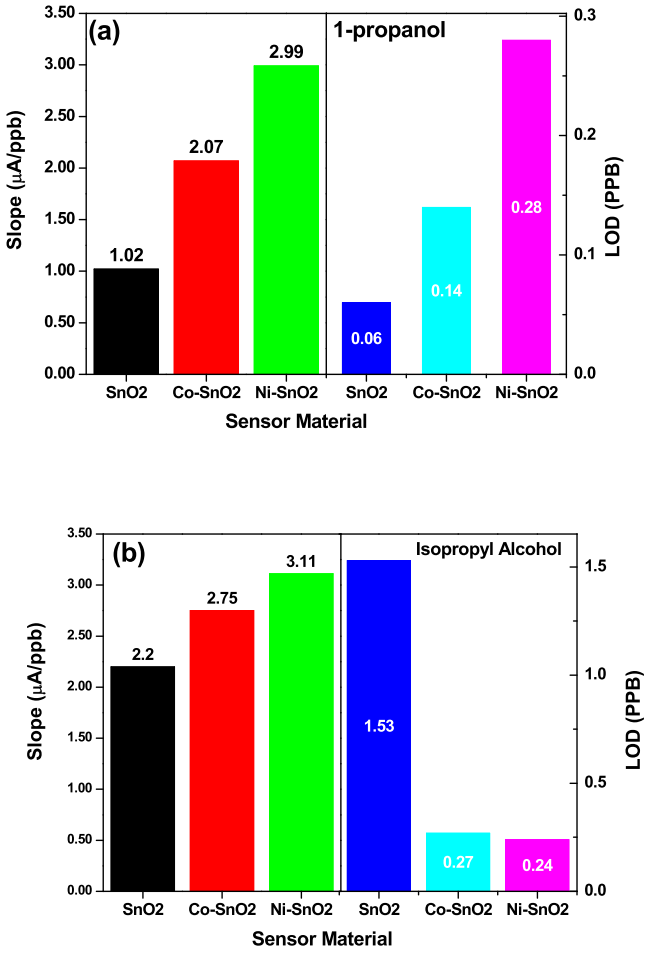

Figure 8. Bar graph showing sensitivity of the developed sensor for (a) 1-propanol and (b) isopropyl alcohol.

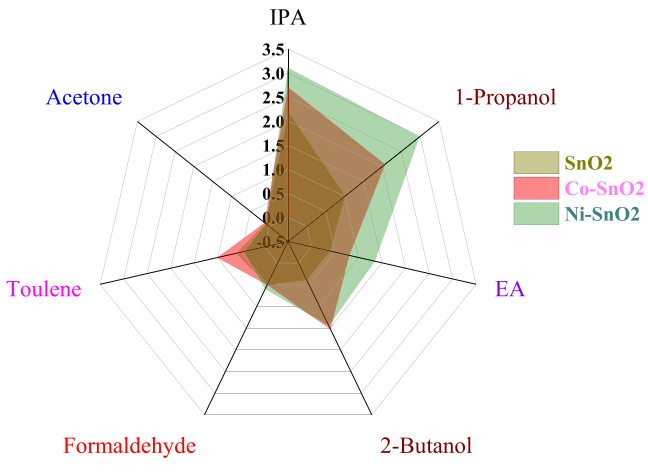

Figure 9. Radar chart showing selectivity of the developed sensor.

is noticed that except acetone, the sensors have significant sensitivity to all the volatile organic compounds tested; however, the difference in sensitivity may be correlated to the different mechanisms involved during the electrochemical interaction of the target on the surface of the sensing electrode like physisorption, chemisorption, charge transfer, and induced dipole scattering.

Theoretically, a critical factor that governs the sensitivity of a material is the ratio between the energy barrier and electron transport between two adjacent grains: SnO_2, and Co and Ni. In general, when the particle size approaches to a nano range, as observed from XRD and FESEM studies, not only the surface or interfaces are influenced but also the entire properties of the particle are dramatically influenced due to the solid−gas/liquid interaction that leads to significant enhancement in sensitivity properties. Thus, it is anticipated that the higher surface area and the nano range of the synthesized material will critically influence the sensitivity of a material. In sync with this mechanism, the material analysis results indicated that the synthesized particles are in a nanometer range (less than 100 nm) and hence provided a higher surface to volume ratio. The FTIR studies also indicated that the synthesized material has functional characteristics to bind with the analyte and thus resulting in better electronic conduction through an electrochemical reaction at the working electrode.

3. DISCUSSION

To analyze the possible reaction mechanism that might be occurring during sensing, the scan rate study of all the sensors was performed by changing the voltage step from 10 to 100 mV/s for both 1-proponal and isopropyl alcohol, and CV curves are shown in Figure S2 (ESI). For 1-propanol (10 ppb), the value of the peak current linearly increases and the oxidation potential is constant for undoped SnO_2 (Figure S2(a)), Co−SnO_2 (Figure S2(b)), and Ni−SnO_2 (Figure S2(c)) sensors. It is expected that during the electrochemical reaction, there could be water hydrolysis resulting in creation of ionic radicals supporting the redox reaction at the electrode surface. The increase of the peak current is correlated to the reduction in depletion resulting in better charge transfer characteristics even at a higher scan rate, whereas the constant redox potential indicates the reaction is diffusion-limited.[31] The linearity of the peak current with the scan rate (Figure S3(a)) is due to the adsorption of the VOC molecule on the surface resulting in rapid charge transfer, in turn, current increases even at a high rate and hence slight nonlinear behavior is observed with the square root of the scan rate (Figure S3(b)) and log[scan rate] (Figure S3(c)). The scan rate study of isopropyl alcohol (6 ppb) reveals a slight redshift of the oxidation potential along with the increase of the peak oxidation current for undoped SnO_2 (Figure S2(d)), Co−SnO_2 (Figure S2(e)), and Ni−SnO_2 (Figure S2(f)). The increase of potential suggests kinetics is slow and reaction time is insufficient at a high scan rate. The graph of the peak oxidation current versus scan rate gives a linear increase of the current with the scan rate, whereas the relation becomes nonlinear with the square root (Figure S3(e)) and/or log of the scan rate (Figure S3(f)). This is correlated to the diffusion-related phenomena on the surface due to adsorbed VOC molecules.[31]

Furthermore, electron transfer properties of the developed sensors were studied by electrochemical impedance spectroscopy (EIS). The charge transport processes in nanosensing electrodes were studied by monitoring the charge transfer resistance (R_{ct}) at the electrode/electrolyte interface. The value of the electron transfer resistance depends on the dielectric and insulating features at the electrode/electrolyte interface. The impedance plot of −Z imaginary part versus Z-real part, i.e., Nyquist plot, is shown in Figures S4 and S5(a). The EIS study of 1-propanol shows maximum R_{ct} values for undoped SnO_2 (Figure S4(a)) and minimum for that of Ni−

https://dx.doi.org/10.1021/acsomega.0c04231
ACS Omega 2020, 5, 27645−27654

SnO_2 (Figure S4 (c)). This is consistent with the CV results that reveal Ni−SnO_2 exhibits the highest sensitivity for 1-propanol (Figures 6 & 8). The increase of the R_{ct} value with the 1-propanol concentration implies the increase of sensor impedance in accordance to the increase of the oxidation current as observed in Figure 6. The EIS study with isopropyl alcohol reveal the general increase of the R_{ct} as a function of concentration for all sensors, i.e., undoped SnO_2 (Figure S4(d)), Co−SnO_2 (Figure S4(e)), and Ni−SnO_2 (Figure S4(f)). The minimum value range of the R_{ct} is almost the same for undoped SnO_2 (Figure S4(d)) and Ni−SnO_2 (Figure S4(f)) as shown in Figure S5(b), whereas the minimum R_{ct} value was observed for Co−SnO_2 (Figure S4(e)).

It is noticed that the R_{ct} value for 1-propanol is comparatively higher for all sensors than that for isopropyl alcohol and may be correlated to the chemical structure of 1-propanol, which can easily lose the proton and oxidize itself and consequently result in the extraction of the electron from the sensor surface.

Based on the CV and EIS study, a possible sensing mechanism is proposed in Figure 10, which presents the

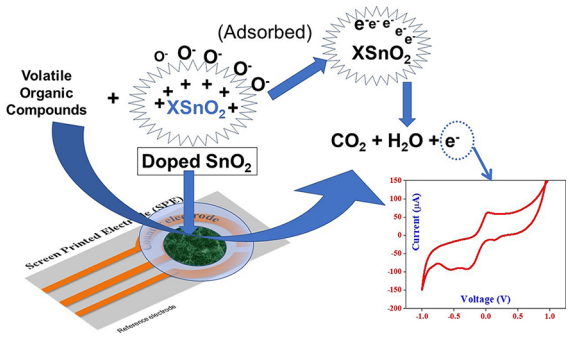

Figure 10. Schematic representation of the proposed sensing setup and mechanism.

sensing mechanism of the VOC in PBS buffer. As the CV curves have been obtained in the buffer solution prior to the VOC test, it is expected that the surface might have an adsorbed oxygen species as a result of water electrolysis during CV. This would facilitate the redox reaction as a function of the VOC and potential. The increase of the oxidative current is therefore observed in the CV study and the increase of R_{ct} in EIS. The higher number of electron transfer will result in the huge reduction of the surface charge density and hence the oxidation current increase with the concentration. On the other hand, during the reduction cycle, surface-adsorbed oxygen will oxidize VOCs into CO_2 and H_2O releasing electron back to the conduction band of the SnO_2 nanomaterial, enhancing the conductivity and sensitivity of the sensor.[32]

In order to check the performance of the developed sensor, we found that Rahman et al. developed an ethanol chemical sensor based on a ternary metal oxide system of CdO/ZnO/Yb_2O_3 nanosheets (NSs) with a sensitivity of 7.4367 μA mM^{-1} cm^{-2} and Ni−SnO_2 nanostructure materials with an approximate sensitivity of 2.3148 μA cm^{-2} mM^{-1} and with a detection limit of 0.6 nM.[33,34] Faisal et al.[35] synthesized ZnO nanoparticles and its methanol sensing characteristics were investigated with an I-V technique with a good sensitivity of 0.9554 μA cm^{-2} mM^{-1}. Wahid et al.[36] used a cobalt oxide-doped neodymium oxide nanocomposite (Co_3O_4@Nd_2O_3 NCs) as a sensor probe material to detect isopropyl alcohol with a sensitivity of 22.152 $nAmM^{-1}$ cm^{-2}. It is realized that the proposed sensor has higher sensitivity than these sensors.

Repeatability, reproducibility, and stability of the developed sensor were also examined. Relative standard deviation (RSD) was calculated to obtain the repeatability parameter for five successive readings/measurements with Co−SnO_2 and Ni−SnO_2 for both 1-propanol and IPA. In the case of Co-doped SnO_2, it was found to be 3.1 and 4.3% for 1-propanol and isopropyl alcohol, respectively; similarly, in the case of Ni doping, repeatability was calculated by RSD, and it was found to be 3.3 and 4% for 1-propanol and isopropyl alcohol, respectively. Also, reproducibility of the experiment was also checked by preparing five different electrodes at different times within 3 months and performing the experiment. The oxidation peak current for each set of electrodes showed RSD of about 5%. This demonstrates that the modified electrode can be easily reproduced.

Stability of the modified electrode was also examined by cyclic voltammetry; in this, we have repeated the CV cycle 50 times for both the doped electrode at a fixed concentration of the analyte. The percent degradation was calculated by dividing the oxidation current obtained from the last cycle, i.e., 50th by the oxidation current of the first cycle and multiplying by 100. The value obtained for the Co−SnO_2 and Ni−SnO_2 modified electrode for both the analyte, i.e., 1 propanol and IPA is ∼1 to 2%. This indicates that the modified electrode is highly stable.

4. MATERIALS AND METHODS

4.1. Materials. Cobalt nitrate hexahydrate ($Co(NO_3)_2 \cdot 6H_2O$) and nickel chloride hexahydrate ($NiCl_2 \cdot 6H_2O$) were purchased from Junsei Chemical Co. Ltd., while tin-tetrachloride pentahydrate ($SnCl_4 \cdot 5H_2O$), 1-propanol (99.7% pure) and isopropyl alcohol (99.5% pure) were purchased from Sigma−Aldrich. The chemicals procured were used as-procured. The double alkali phosphate buffer saline (pH = 7.0, 0.1 M PBS) was used as the reference/supporting medium prepared with monosodium phosphate (0.1 M) and disodium phosphate (0.1 M) mixed in an equal ratio in millipore water. Furthermore, using this PBS, we prepared different concentrations of 1-propanol and isopropyl alcohol. Stock solution of 1-propanol was prepared by taking 1 μL of 1-propanol in 1 L of PBS. Different concentrations of 1-propanol (0, 1, 5, 10, and 15 ppb) were prepared by using the $C_1V_1 = C_2V_2$ formula. Similarly, a stock solution of 1 ppm of isopropyl alcohol was prepared and diluted with PBS to make different concentrations of isopropyl alcohol (0, 2, 4, 6, 8, and 10 ppb), respectively.

4.2. Methods. Tin oxide nanoparticle synthesis was carried out using the sol−gel method. In a typical reaction, 3.51 g of $SnCl_4 \cdot 5H_2O$ was dissolved in 50 mL of DI water to get a 0.1 M solution, stirred on a magnetic stirrer. During stirring, an aqueous ammonia solution (0.1 M) was added dropwise until thin gel was precipitated. The solution was then washed several times with deionized water till neutral pH was obtained; this also removed unreacted ions and excess ammonia. The obtained precipitate was dried at 70 °C followed by calcination at 800 °C.

For doping with Co, a 0.1 M solution of copper nitrate hexahydrate ($Co(NO_3)_2 \cdot 6H_2O$) was prepared by adding 1.455 mg in 50 mL of water, which was then mixed into the 50 mL SnO_2 solution (0.1 M). Stirring was done with the dropwise

https://dx.doi.org/10.1021/acsomega.0c04231
ACS Omega 2020, 5, 27645−27654

addition of aqueous ammonia till a greenish colloidal gel is formed. Final precipitate was washed several times, dried, and calcined as undoped SnO_2.

For doping with nickel, the similar procedure was followed with 0.1 M of nickel chloride hexahydrate ($NiCl_2{\cdot}6H_2O$, 1.18 mg) in 50 mL of water. A greenish colloidal gel was formed, which was further followed by several washing, drying, and calcination at 800 °C.

The morphological analysis of as-synthesized nanoparticles was carried out using Hitachi's S5200 FESEM at an acceleration voltage of 10 keV. Structural characterizations were carried out using an X-ray diffractometer (Rigaku, Ultima IV) with Cu Kα radiation (λ = 1.542 Å), and the diffraction pattern was recorded over the Bragg's angle between 20 to 80°. Surface functional analysis was done with Fourier transform infrared spectroscopy (FTIR, Bruker's Tensor 37 spectrometer), and spectra is obtained in the frequency range of 600 to 4000 cm^{-1}; UV−vis absorption studies were done in the wavelength range of 200 to 600 nm using the Hitachi's U3900 spectrophotometer.

For the prefabricated three terminals (counter, reference, and working electrodes), a gold-coated Cu- electrode was used to prepare a screen-printed electrode (SPE) as an electrochemical sensor platform. Thick film of the calcined nanoparticle was printed on the working electrode having 4 mm in diameter and was dried at 70 °C. Such SPE was printed with undoped and doped SnO_2 nanomaterials separately.

Electrochemical characterization, i.e., cyclic voltammetry (CV) and electrochemical impedance spectroscopy (EIS) was performed using a potentiostat (IVIUM, Netherland) with printed SPEs. The voltammogram was obtained by sweeping the voltage between −1 V to +1 V at a scan rate of 100 mV per s, whereas the EIS spectra were recorded in the frequency range of 1 MHz to 0.1 Hz. The characterization was repeated for all the samples and for different concentrations (0, 1, 5, 10, and 15 ppb) of 1-propanol solution and (0, 2, 4, 6, 8, and 10 ppb) of isopropyl alcohol (IPA), which were prepared in the phosphate buffer solution. For an actual measurement, the breath sample can be transported through a condenser to the sample vial containing PBS, and then the measurement can be performed.

5. CONCLUSIONS

In this work, an attempt is made to study an e-nose based concept by using undoped, Co-, and Ni-doped SnO_2 nanoparticles in the form of an SPE for 1-propanol (0 to 15 ppb) and isopropyl alcohol (0 to 10 ppb) detection. Morphology of the synthesized nanoparticles was confirmed by the FESEM, whereas XRD revealed the crystalline structure. Ni-doped SnO_2 resulted in the highest sensitivity for both analytes within the detection range. From selectivity studies, it is noticed that Ni−SnO_2 offers the highest selectivity for IPA against all other volatile compounds analyzed. Co−SnO_2 exhibits the highest selectivity to 1-propanol against all the volatile compounds tested. The results of this study indicate that these doped SnO_2 can be used as a potential sensing platform for the detection of various VOCs in an attempt for early/timely detection of lung cancer.

ASSOCIATED CONTENT

Supporting Information

The Supporting Information is available free of charge at https://pubs.acs.org/doi/10.1021/acsomega.0c04231.

Contact angle images, CV curves as a function of different scan rates at 10ppb of 1-propanol, redox peak currents, EIS curves at a fixed concentration, EIS curves for the change in R_{ct} values with changing concentration (PDF)

AUTHOR INFORMATION

Corresponding Authors

Hassan Fouad − *Applied Medical Science Dept., Community College, King Saud University, Riyadh 11433, Saudi Arabia; Biomedical Engineering Department, Faculty of Engineering, Helwan University, Helwan 11792, Egypt*; Email: menhfef@ksu.edu.sa

Shafeeque Ahmed Ansari − *Centre for Interdisciplinary Research in Basic Science, Jamia Millia Islamia, New Delhi 110025, India*; orcid.org/0000-0002-1384-0143; Email: saansari@jmi.ac.in

Authors

Zeenat Khatoon − *Centre for Interdisciplinary Research in Basic Science, Jamia Millia Islamia, New Delhi 110025, India*

Othman Y. Alothman − *Chemical Engineering Department, College of Engineering, King Saud University, Riyadh 11451, Saudi Arabia*

Mohamed Hashem − *Dental Health Department, College of Applied Medical Sciences, King Saud University, Riyadh 11433, Saudi Arabia*

Zubaida A. Ansari − *Centre for Interdisciplinary Research in Basic Science, Jamia Millia Islamia, New Delhi 110025, India*

Complete contact information is available at: https://pubs.acs.org/10.1021/acsomega.0c04231

Author Contributions

Z.A.A. and S.A.A.conceptualized the study and provided resources. Z.K. and S.A.A. performed the methodology and data curation. Z.K. performed the software analysis and investigation. Z.K., H.F., M.H., and O.Y.A participated in the validation, writing, and preparation of the original draft. Z.K. & H.F. performed the formal analysis. Z.A.A., H.F. took part in writing and the review and editing of the paper. S.A.A. supervised and was part of the project administration. All authors have read and agreed to the published version of the manuscript.

Funding

The authors extend their appreciation to the Deputyship for Research & Innovation, "Ministry of Education" in Saudi Arabia for funding this research work through the project number IFKSURG-1435-052.

Notes

The authors declare no competing financial interest.

Authors appreciate the measurement support received from the Central Instrumentation Facility and DST-PURSE Program of Jamia Millia Islamia, New Delhi.

REFERENCES

(1) Poli, D.; Carbognani, P.; Corradi, M.; Goldoni, M.; Acampa, O.; Balbi, B.; Bianchi, L.; Rusca, M.; Mutti, A. Exhaled volatile organic compounds in patients with non-small cell lung cancer: cross sectional and nested short-term follow-up study. *Respir. Res.* **2005**, *6*, 71.

(2) Makar, A. B.; McMartin, K. E.; Palese, M.; Tephly, T. R. Formate assay in body fluids: application in methanol poisoning. *Biochem. Med.* **1975**, *13*, 117−126.

(3) Wang, Y.; Hu, Y.; Wang, D.; Yu, K.; Wang, L.; Zou, Y.; Zhao, C.; Zhang, X.; Wang, P.; Ying, K. The analysis of volatile organic compounds biomarkers for lung cancer in exhaled breath, tissues and cell lines. *Cancer Biomark* **2012**, *11*, 129−137.
(4) Basanta, M.; Ibrahim, B.; Dockry, R.; Douce, D.; Morris, M.; Singh, D.; Woodcock, A.; Fowler, S. J. Exhaled volatile organic compounds for phenotyping chronic obstructive pulmonary disease: a cross-sectional study. *Respir. Res.* **2012**, *13*, 72.
(5) Chatterjee, S.; Castro, M.; Feller, J. F. An e-nose made of carbon nanotube based quantum resistive sensors for the detection of eighteen polar/nonpolar VOC biomarkers of lung cancer. *J. Mater. Chem. B* **2013**, *1*, 4563.
(6) Peng, G.; Trock, E.; Haick, H. Detecting Simulated Patterns of Lung Cancer Biomarkers by Random Network of Single-Walled Carbon Nanotubes Coated with Nonpolymeric Organic Materials. *Nano Lett.* **2008**, *8*, 3631−3635.
(7) Peled, N.; Barash, O.; Tisch, U.; Ionescu, R.; Broza, Y. Y.; Ilouze, M.; Mattei, J.; Bunn, P. A., Jr.; Hirsch, F. R.; Haick, H. Volatile fingerprints of cancer specific genetic mutations. *Nanomedicine* **2013**, *9*, 758−766.
(8) Callol-Sanchez, L.; Munoz-Lucas, M. A.; Gomez-Martin, O.; Maldonado-Sanz, J. A.; Civera-Tejuca, C.; Gutierrez-Ortega, C.; et al. Observation of nonanoic acid and aldehydes in exhaled breath of patients with lung cancer. *J. Breath Res.* **2017**, *11*, No. 026004.
(9) Oguma, T.; Nagaoka, T.; Kurahashi, M.; Kobayashi, N.; Yamamori, S.; Tsuji, C.; Takiguchi, H.; Niimi, K.; Tomomatsu, H.; Tomomatsu, K.; et al. Clinical contributions of exhaled volatile organic compounds in the diagnosis of lung cancer. *PloS one* **2017**, *12*, No. e0174802.
(10) Chow, Y. W.; Pietranico, R.; Mukerji, A. Studies of oxygen binding energy to hemoglobin molecule. *Biochem. Biophys. Res. Commun.* **1975**, *66*, 1424−1431.
(11) Deng, Y.; Sun, J.; Jin, H.; Khatib, M.; Li, X.; Wei, Z.; Wang, F.; Horev, Y. D.; Wu, W.; Haick, H. Chemically Modified Polyaniline for the Detection of Volatile Biomarkers of Minimal Sensitivity to Humidity and Bending. *Adv. Healthcare Mater.* **2018**, *7*, 1800232.
(12) Hakim, M.; Broza, Y. Y.; Barash, O.; Peled, N.; Phillips, M.; Amann, A.; Haick, H. Volatile Organic Compounds of Lung Cancer and Possible Biochemical Pathways. *Chem. Rev.* **2012**, *112*, 5949−5966.
(13) Kusano, M.; Mendez, E.; Furton, K. G. Development of headspace SPME method for analysis of volatile organic compounds present in human biological specimens. *Anal. Bioanal. Chem.* **2011**, *400*, 1817−1826.
(14) Di Francesco, F.; Fuoco, R.; Trivella, M. G.; Ceccarini, A. Breath analysis, trends in techniques and clinical applications. *Microchem. J.* **2005**, *79*, 405−410.
(15) Hryniuk, A.; Ross, B. M. Detection of acetone and isoprene in human breath using a combination of thermal desorption and selected ion flow tube mass spectrometry. *Int. J. Mass Spectrom.* **2009**, *285*, 26−30.
(16) Jones, A. W.; Lagesson, V.; Tagesson, C. Determination of isoprene in human breath by thermal desorption gas chromatography with ultraviolet detection. *J. Chromatogr. B: Biomed. Sci. Appl.* **1995**, *672*, 1−6.
(17) Hyšpler, R.; Crhová, Š.; Gasparič, J.; Zadák, Z.; Čížková, M.; Balasová, V. Determination of isoprene in human expired breath using solid-phase microextraction and gas chromatography−mass spectrometry. *J. Chromatogr. B: Biomed. Sci. Appl.* **2000**, *739*, 183−190.
(18) Rudnicka, J.; Kowalkowski, T.; Ligor, T.; Buszewski, B. Determination of volatile organic compounds as biomarkers of lung cancer by SPME−GC−TOF/MS and chemometrics. *J. Chromatogr., B* **2011**, *879*, 3360−3366.
(19) Abbott, S. M.; Elder, J. B.; Španěl, P.; Smith, D. Quantification of acetonitrile in exhaled breath and urinary headspace using selected ion flow tube mass spectrometry. *Int. J. Mass Spectrom.* **2003**, *228*, 655−665.
(20) Storer, M.; Salmond, J.; Dirks, K. N.; Kingham, S.; Epton, M. Mobile selected ion flow tube mass spectrometry (SIFT-MS) devices and their use for pollution exposure monitoring in breath and ambient air−pilot study. *J. Breath Res.* **2014**, *8*, No. 037106.
(21) King, J.; Mochalski, P.; Kupferthaler, A.; Unterkofler, K.; Koc, H.; Filipiak, W.; Teschl, S.; Hinterhuber, H.; Amann, A. Dynamic profiles of volatile organic compounds in exhaled breath as determined by a coupled PTR-MS/GC-MS study. *Physiol. Meas.* **2010**, *31*, 1169−1184.
(22) Zhan, X.; Duan, J.; Duan, Y. Recent developments of proton-transfer reaction mass spectrometry (PTR-MS) and its applications in medical research. *Mass Spectrom. Rev.* **2013**, *32*, 143−165.
(23) Mochalski, P.; Rudnicka, J.; Agapiou, A.; Statheropoulos, M.; Amann, A.; Buszewski, B. Near real-time VOCs analysis using an aspiration ion mobility spectrometer. *J. Breath Res.* **2013**, *7*, No. 026002.
(24) Broza, Y. Y.; Vishinkin, R.; Barash, O.; Nakhleh, M. K.; Haick, H. Synergy between nanomaterials and volatile organic compounds for non-invasive medical evaluation. *Chem. Soc. Rev.* **2018**, *47*, 4781−4859.
(25) Broza, Y. Y.; Mochalski, P.; Ruzsanyi, V.; Amann, A.; Haick, H. Hybrid Volatolomics and Disease Detection. *Angew. Chem., Int. Ed.* **2015**, *54*, 11036−11048.
(26) Přech, J.; Pizarro, P.; Serrano, D. P.; Čejka, J. From 3D to 2D zeolite catalytic materials. *Chem. Soc. Rev.* **2018**, *47*, 8263−8306.
(27) Comini, E. Metal oxide nano-crystals for gas sensing. *Anal. Chim. Acta* **2006**, *568*, 28−40.
(28) Kim, H.-J.; Lee, J.-H. Highly sensitive and selective gas sensors using p-type oxide semiconductors: Overview. *Sens. Actuators, B* **2014**, *192*, 607−627.
(29) Soussi, L.; Garmim, T.; Karzazi, O.; Rmili, A.; El Bachiri, A.; Louardi, A.; Erguig, H. Effect of (Co, Fe, Ni) doping on structural, optical and electrical properties of sprayed SnO_2 thin film. *Surf. Interfaces* **2020**, *19*, 100467.
(30) Suman, P. H.; Felix, A. A.; Tuller, H. L.; Varela, J. A.; Orlandi, M. O. Comparative gas sensor response of SnO_2, SnO and Sn_3O_4 nanobelts to NO_2 and potential interferents. *Sens. Actuators, B* **2015**, *208*, 122−127.
(31) Bard, A. J.; Faulkner, L. R. *Electrochemical methods fundamentals and applications*; 2nd ed.; John Wiley & Sons, Inc.: New York, 2001.
(32) Ansari, S. G.; Fouad, H.; Shin, H.-S.; Ansari, Z. A. Electrochemical enzyme-less urea sensor based on nano-tin oxide synthesized by hydrothermal technique. *Chem.-Biol. Interact.* **2015**, *242*, 45−49.
(33) Rahman, M. M.; Alam, M. M.; Asiri, A. M.; Islam, M. A. Ethanol sensor development based on ternary-doped metal oxides ($CdO/ZnO/Yb_2O_3$) nanosheets for environmental safety. *RSC Adv.* **2017**, *7*, 22627−22639.
(34) Rahman, M. M.; Jamal, A.; Khan, S. B.; Faisal, M. Highly sensitive ethanol chemical sensor based on Ni-doped SnO_2 nanostructure materials. *Biosens. Bioelectron.* **2011**, *28*, 127−134.
(35) Faisal, M.; Khan, S. B.; Rahman, M. M.; Jamal, A.; Abdullah, M. M. Fabrication of ZnO nanoparticles based sensitive methanol sensor and efficient photocatalyst. *Appl. Surf. Sci.* **2012**, *258*, 7515−7522.
(36) Wahid, A.; Asiri, A. M.; Rahman, M. M. Fabrication of an efficient Isopropyl alcohol sensor based on facile Co_3O_4@Nd_2O_3 nanocomposites for environmental safety. *Environ. Nanotechnol., Monit. Manage.* **2018**, *10*, 314−321.

https://dx.doi.org/10.1021/acsomega.0c04231
ACS Omega 2020, 5, 27645−27654